J. Fluid Mech. (1987), vol. 181, pp. 441–466
Printed in Great Britain

Numerical simulation of compressible homogeneous flows in the turbulent regime

By T. PASSOT AND A. POUQUET
Observatoire de Nice, B.P. 139, Nice CEDEX 06003, France

(Received 14 July 1986)

Compressible flows with r.m.s. velocities of the order of the speed of sound are studied with direct numerical simulations using a pseudospectral method. We concentrate on turbulent homogeneous flows in the two-dimensional case. The fluid obeys the Navier–Stokes equations for a perfect gas, and viscous terms are included explicitly. No modelling of small scales is used. We show that the behaviour of the flow differs sharply at low compared with high r.m.s. Mach number Ma, with a transition at $Ma = 0.3$. In the large scales, temporal exchanges between longitudinal and solenoidal modes of energy retain an acoustical character; they lead to a slowing down of the decrease of the Mach number with time, which occurs with interspersed plateaux corresponding to quiescent periods. When the flow is initially supersonic, the small scales are dominated by shocks behind which vortices form. This vortex production is particularly prominent when two strong shocks collide, with the onset of shear turbulence in the region downstream of the collision. However, at the resolutions reached by our code on a 256×256 uniform grid, this mechanism proves insufficient to bring vortices into equipartition with shocks in the small-scale tail of the energy spectrum.

1. Introduction

There are many examples of fluids around us that are compressible, at least enough to allow for sound propagation. On the other hand, flows in which the fluctuating Mach number is important are encountered in the fields of aerodynamics (for example, problems concerning the re-entry into the atmosphere of shuttle-like vehicles, or concerning the concept of the scramjet), as well as in astrophysics. Indeed, many celestial observations point to supersonic flows, in accretion disks, in galactic and extra-galactic jets and in molecular clouds. In the latter case, recent data obtained in radio astronomy for CO lines and H_2CO lines reveal an heterogeneous structure, consisting of bubbles with a turbulence among them having a velocity dispersion greater than the sound speed. Moreover, such a turbulence seems to follow a Kolmogorov law (Larson 1981), although somewhat steeper (M. Perault 1986, paper in preparation). The origin of such turbulence, in which self-gravitation plays a central role, is disputed and may be linked, for example, to stellar winds or to the presence of magnetic fields. In all instances, the flows may be considered homogeneous on average.

Compressible flows have been studied extensively in the acoustic regime and many problems have been treated: how does noise affect the primary flow, and vice versa (Yates 1978)? What is the sound emitted in the far-field regime (Lighthill 1952, 1954; Crighton 1975)? How is the Kolmogorov law of spectral distribution of energy with

scale affected by a small density fluctuation? On the other hand, in the fully nonlinear regime, few analytical techniques are available. The approach of the renormalization group is rendered difficult by the high degree of nonlinearity of the equations (except in the acoustic case). Another possible technique is that of homogenization (Chacon & Pironneau 1986). For the one-dimensional problem, Tatsumi & Tokunaga (1974) showed that the long-time large-scale properties of a weakly compressible flow are described by the Burgers' equation.

In the laboratory, the Lighthill formula for sound emission is verified up to Mach numbers well above the acoustic regime, the precise value depending upon the geometry of the flow. However, experiments in the regimes of interest to aerodynamicists and astrophysicists with a supersonic fluctuating Mach number are almost non-existent. In this context, numerical simulations are particularly useful. Many studies have been devoted to the inviscid problem, using a variety of artificial viscosities within the shocks (Roache 1972). Few codes, however, deal with the full Navier–Stokes equations which smooth the shocks naturally with no special restriction. Spectral methods have been widely used in the incompressible case and are now being extended to the compressible one (Streett, Zang & Hussaini 1983; Léorat & Pouquet 1986). Such methods, known for their accuracy for smooth flows (Gottlieb & Orszag 1977), are simple to implement in particular when the flow is assumed to be homogeneous. One-dimensional studies have shown that, even in the presence of shocks, spectral methods contain phase information that allows one to reconstruct the position of the shock (Arbarbanel, Gottlieb & Tadmor 1985). Studies of three-dimensional compressible viscous flows have been limited to a few cases (Feiereisen, Reynolds & Ferziger 1981) due to the limitation in resolution on present-day computers.

In this paper, we present numerical results obtained for an homogeneous compressible fluid following the perfect-gas law and restricted to evolution in a plane. We choose to solve the Navier–Stokes equation, with dissipation terms treated explicitly and thus naturally smoothing shocks that will form. The main questions we address concerns the distribution of energy among the modes (compressible, solenoidal, internal) as a function of the scale, and the lifetime of a supersonic turbulence. We describe the numerical method in §2 and the results at low Mach number in §3 and at high Mach number in §4. Long-time properties of the flow are described in §5 and conclusions are presented in §6.

2. The numerical method

2.1. *Introduction*

We shall describe the method we use in reasonable detail since our choice is not the usual one for compressible flows.

In order to achieve good precision in the computation of the flow evolution, including the small scales, spectral methods are known to be both efficient and simple to implement. In particular, they are well adapted to homogeneous flows for which one can use periodic boundary conditions with a Fourier representation. We thus develop in Fourier series each of the variable fields (see the equations below) in a square domain of $N \times N$ points uniformly distributed. Space differentiations are performed in spectral space, in which they reduce to simple multiplications, whereas the nonlinear terms are evaluated in configuration space. The method is efficient because there are now fast Fourier transform (FFT) algorithms written in machine

language; the one we use is due to C. Temperton, and allows the number of (linear) grid points N to be written as

$$N \sim 2^a 3^b 5^d.$$

Our purpose is to reach the highest Reynolds number possible in order to let the flow develop turbulent structures. In order to do so, we have to adapt the code to the computer we use, the CRAY-1 of CCVR. It consists of one processor with 1 Mword of 64 bits (in fact, slightly more) in the central memory and a cycle time of 12.5 ns. On such a machine, which is fast but with (relatively speaking) little memory, we choose to minimize the number of $N \times N$ arrays used, at the cost of extra FFTs to compute the various terms of the equations. We thus use 14 N × N arrays altogether and 19 FFTs are computed per time-step. It should be noted that in the barotropic case, where the pressure is a function of density, the number of FFTs can be as low as 8. The equations are written in conservation form (see below) which makes the temporal conservation of mass, momentum and total energy particularly simple to implement with a spectral method. We stress that the dissipative terms are treated in an exact way, with no approximation, which accounts for the fact that the computation of the energy equation is costly. No filtering in the smallest scales of the flow is used either, which will show up in the contour of the derivative fields such as the vorticity. It is known that, in the presence of a sharp discontinuity, the Gibbs phenomenon occurs, with oscillations at the edge of the jump that do not disappear as the number of modes is increased in the computation. It has been shown (Abarbanel *et al.* 1985) on one-dimensional computations that such oscillations should not in fact be filtered out, since they contain phase information essential in localizing the shock position. However, we choose to simulate not the Euler equations but the Navier–Stokes equations, in which case we have to adapt the viscosity in order that the quasi-discontinuity in velocity (for example) is spread out over several grid points. Here we have some latitude, depending on what the computation is aimed at. When we wish to stress the large-scale phenomena, three grid points per jump appears to be the limit before instabilities develop, but displays of vorticity or similar fields will show strong oscillations of the Gibbs type. On the other hand, to perform predictions on the behaviour of the flow in the small scales, as many as eight grid points through the pseudoshock may be necessary.

With nonlinear dissipative terms, we make use of an entirely explicit temporal scheme, namely the Adams–Bashforth one which is second-order accurate in time. Two stability conditions arise, which we recall here. The first one is that of Courant–Friedrichs–Levy (CFL):

$$\Delta t < \frac{1}{k_{\max}\|U_{\max}| + |C_{\max}\|}, \tag{2.1}$$

where Δt is the time-step, $k_{\max}$ the high-cutoff wavenumber of the computation, and $U_{\max}$ and $C_{\max}$ are the maxima of the velocity and of the speed of sound respectively. The other stability criterion is related to the viscous terms, and reads

$$\Delta t < \frac{1}{\mu k_{\max}^2 |\rho_{\min}|^{-1}}, \tag{2.2}$$

where μ is the dynamic viscosity and $\rho_{\min}$ the density minimum (taken over the computation box). It is the latter condition that imposes the most severe constraint on the possible time-step we use at high Mach number, because of cavitation effects

with the occurrence of regions of very low density; it is the former constraint that matters at low Mach number since the sound speed is high (or conversely the typical velocities are low).

The code has been run on the CRAY 1 of the CCVR with a resolution of up to 256×256 grid points. One time-step is performed in 0.6 s of CPU time, and the memory necessary for the code is 1.2 Mwords. We were led to make use of peripheral memory to achieve such a resolution, with an additional cost because of the slow transfer time with central core.

A typical run lasts three hours of CPU at that resolution. This shows the limitations of machines such as the CRAY 1 and it is the main reason for our using the two-dimensional approximation. The three-dimensional case awaits the arrival of more powerful computers which will probably be multi-processors.

2.2. *The equations in nondimensionalized form*

We consider a medium of characteristic length L, of mean density ρ_0 and mean velocity U_0. The density ρ and the velocity $\boldsymbol{u}$ are normalized to unity through the introduction of these mean values, and the spatial scale (size of the computation box) is 2π, with wavenumbers varying from $k_{\min} = 1$ to $k_{\max} = \frac{1}{2}N$ with N the number of grid points used in each direction (we choose square boxes). We still have to determine, in the framework of classical mechanics, a temperature scale. In the definition of the Mach number $M = U_0/C_0$, the sound velocity is based on the normalization temperature T_0: indeed $C_0^2 = \gamma R T_0$, where γ is the adiabatic index and R the perfect-gas constant. T_0 is chosen to ensure that the temperature variable T also be of order unity. Taking, furthermore, as dependent units L/U_0 for time and U_0^2 for internal energy, the Navier–Stokes equations, with a perfect-gas law, take the form

$$\partial_t \rho + \boldsymbol{\nabla}\cdot(\rho \boldsymbol{u}) = 0, \tag{2.3}$$

$$\partial_t \rho \boldsymbol{u} + \boldsymbol{\nabla}\cdot(\rho \boldsymbol{u}\boldsymbol{u}) = -(\gamma-1)\,\boldsymbol{\nabla}(\rho e) + \frac{1}{Re}(\nabla^2 \boldsymbol{u} + \tfrac{1}{3}\boldsymbol{\nabla}(\boldsymbol{\nabla}\cdot\boldsymbol{u})), \tag{2.4}$$

$$\partial_t E + \boldsymbol{\nabla}\cdot(E\boldsymbol{u} + (\gamma-1)\rho e \boldsymbol{u}) = \frac{1}{Re}\boldsymbol{\nabla}\cdot(\boldsymbol{\tau}\cdot\boldsymbol{u}) + \frac{1}{(\gamma-1)\,Pr\,Re\,M^2}\nabla^2 T, \tag{2.5}$$

where three dimensionless parameters appear: the Mach number $M = U_0/C_0$, the Reynolds number $Re = \rho_0 U_0 L/\mu$ and the Prandtl number $Pr = \mu C_p/\kappa$ where C_p is the constant-pressure specific heat and κ is the coefficient of thermal conductivity. In the above equations, $e = C_v T$ is the internal energy where C_v is the constant-volume specific heat, and $E = \rho e \pm \frac{1}{2}\rho u^2$ is the total energy. Finally τ_{ij} is the viscous stress tensor, defined as

$$\tau_{ij} = \eta \boldsymbol{\nabla}\cdot\boldsymbol{u}\delta_{ij} + \mu(\partial_j u_i + \partial_i u_j), \tag{2.6}$$

where δ_{ij} is the Kronecker symbol and where $\eta = -\frac{2}{3}\mu$, with the choice of a zero volumetric viscosity coefficient. These equations conserve mass, momentum and total energy. In the barotropic case ($p = \rho^\alpha$), the potential vorticity ω/ρ (where $\omega = \operatorname{curl}\boldsymbol{u}$) is a Lagrangian invariant. In the thermodynamic case, only a weaker conservation, namely that of total vorticity obtains (Gaffet 1985), and thus potential-enstrophy conservation is lost. Note that in geostrophic turbulence, for small perturbations, one can make use of quasi-conservation of enstrophy (Farge & Sadourny 1987). In our case, fluctuations in the density field are strong enough to prevent any analysis in such terms.

2.3. *Initial conditions*

In the computations described in this paper, we systematically use random initial conditions in order not to introduce an experimental bias. This is done by computing with a random-number generator the Fourier components of the four scalar fields. In each field, we then multiply the components enclosed in a cylindrical layer of width unity and of wavenumber labelled by a given k_1, by a constant $c(k_1)$ to obtain a field, the correlation spectrum of which we can prescribe at will. We take

$$c(k) \sim k^4 \exp\left(\frac{-2k^2}{k_0^2}\right), \tag{2.7}$$

where k_0 is the wavenumber corresponding to the integral scale of the flow $l_0 \sim k_0^{-1}$. The above choice is customary in turbulence simulations, and corresponds to initial conditions mimicking a noisy large-scale instability with exponential fall-off. For the density and the temperature fields, we need to deal with configuration-space data to impose positivity everywhere, as well as unit mean value and the given correlation. For the velocity, we decompose the randomly produced field into its zero divergence part $\boldsymbol{u}_s$, and zero-curl part $\boldsymbol{u}_c$ by simply making a projection of its Fourier components respectively parallel and perpendicular to the wavevector. This decomposition is particularly well-suited to the spectral method used here and is furthermore convenient for stressing the new features that develop in the flow, when compared to the incompressible case.

The degrees of freedom of given initial conditions are thus taken to be the integral scale k_0^{-1}, the energy ratio between the two velocity modes (compressible and solenoidal), the intensity of density and temperature fluctuations, the fluctuating Mach number of the flow, the Reynolds number, chosen so as to ensure proper dissipation in the small scales (the values given in this paper are based on the Taylor microscale), the Prandtl number, which we keep constant and equal to unity throughout the paper, and finally, the adiabatic index γ which we also fix here to be 1.4. With a 256×256 code, a Reynolds number of 500 or Mach numbers (based on the fluctuating velocity field) of up to 2, on average, are reached.

2.4. *Tests of the code*

Apart from trivial tests, such as computing the first time-step by hand with simple initial conditions and comparing it to the numerical output, we have performed one-dimensional shock-tube calculations to verify the accuracy of the code. These tests are reported elsewhere (Léorat, Pouquet & Poyet 1984) for the barotropic case, with polytropic indices of 1.4 and 1, and an initial density jump of 8. We show in figure 1 the results of a calculation of a shock tube in the thermodynamic case. The gas is initially at rest with constant temperature $T_1 = 1$; the density presents two jumps separating three constant states, the middle one ($\rho_4 = 3$) being ten times denser than the other two. We in fact simulate two shock tubes in order to satisfy the periodic boundary conditions. The initial discontinuity degenerates into a shock wave (with height ρ_2, U_2 and T_2) propagating with velocity s, and a rarefaction wave. The two opposite-travelling waves are separated by a contact discontinuity with height ρ_3 and T_3. The computation is done on a grid with 256 points; the dynamical viscosity is 5×10^{-3} and the Prandtl number here is taken infinite.

In table 1, we compare the values of the jumps given analytically to those found in the numerical simulation. The agreement is better than 0.5 %. We note that the

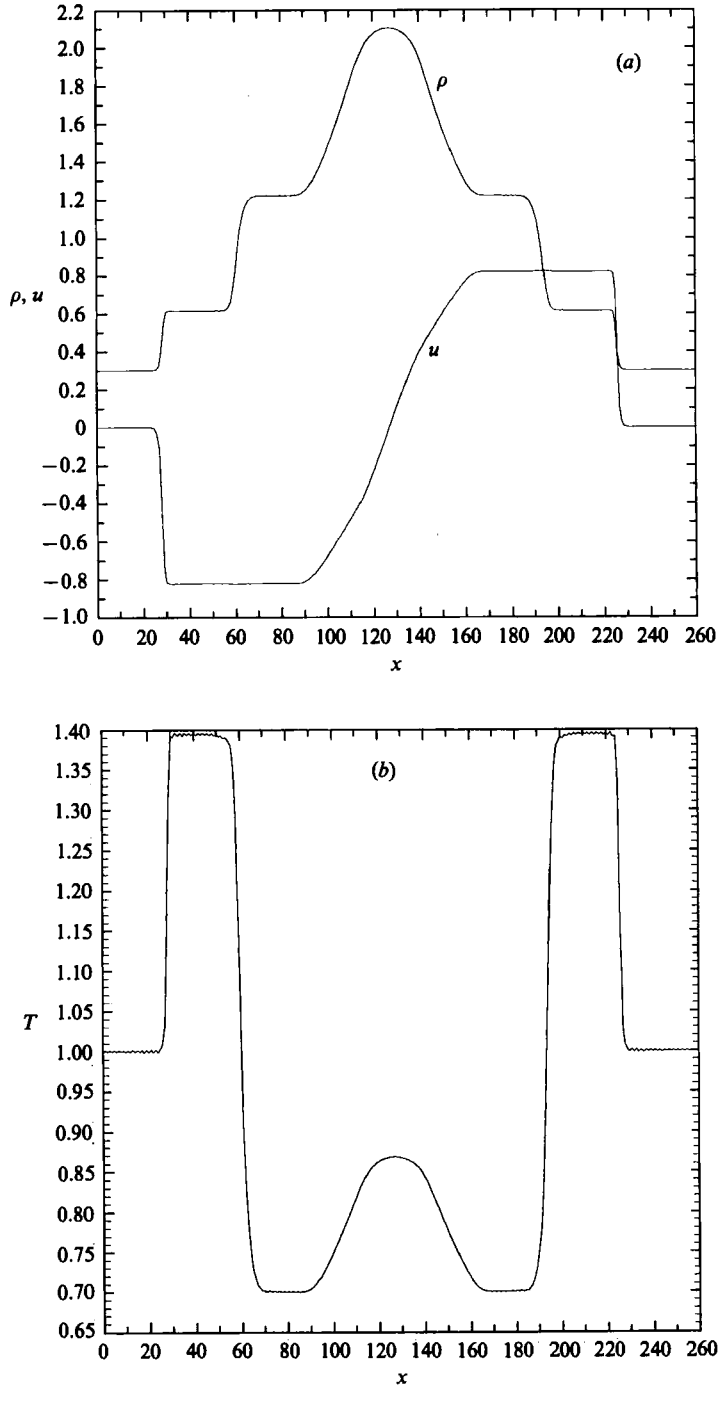

FIGURE 1. Shock-tube simulation for $\gamma = 1.4$ on a 256 point grid. The dynamical viscosity is 5×10^{-3} and the Prandtl number is infinite; (*a*) density and velocity; (*b*) temperature.

	ρ_2	ρ_3	T_2	T_3	U_2	s
Predicted	0.613	1.223	1.393	0.698	0.821	1.608
Observed	0.616	1.218	1.395	0.70	0.821	1.595

TABLE 1. Comparison between predicted and observed values for the parameters of the shock tube; s is the velocity of the shock. Both agree to within less than 0.5%.

Run	N	Re $t=0$	Ma $t=0$	χ $t=0$	Re $t=2$	Ma $t=2$	χ $t=2$	k_0
A	128	50	0.028	0.07	56	0.037	0.65	3.7
B	256	115	1.65	0.12	76	1.10	0.20	1.8
C	256	300	1.10	0.58	215	0.81	0.50	1.2

TABLE 2. Characteristics of runs described in this paper. N is the linear resolution, Re the Reynolds number based on the Taylor microscale, Ma the r.m.s. Mach number, $\chi = E^c/E^v$ the ratio of the compressible to the kinetic energy, and k_0 the wavenumber corresponding to the integral scale. For all two-dimensional runs, the Prandtl number is unity, $\gamma = 1.4$ and the mean density and temperature are equal to one. Initial conditions are random with the given spectrum peaking at k_0 with an exponential fall-off at small scales.

contact discontinuity extends over more points than the shock wave (9 versus 4), this effect being amplified when the Prandtl number is not infinite.

Finally, the labels of the various runs described in this paper are given in table 2 with some of their characteristics.

3. The weak Mach-number regime

Although the code is set-up to study the case where the Mach number is close to unity, we start the description of our results by stating how the flow is modified when compressibility effects are taken into account, first at a low level. We thus take initial conditions that are close to the incompressible case. Two regimes appear, according to whether the density fluctuations $\delta\rho/\rho$ at $t = 0$ are larger or smaller than Ma^2.

When, initially, $\delta\rho/\rho \leqslant Ma^2$ the regime remains quasi-incompressible for all times. Most of the energy is in the solenoidal part at all scales, with the ratio between the divergence-free and the curl-free energy spectrum increasing with wavenumber. We make no attempt to perform a detailed study of inertial indices m of the spectra, defined via

$$E(k) \sim k^{-m}, \tag{3.1}$$

but rather evaluate them in a simple way. The reason is that, even in a 256×256 computation, the inertial range is limited to at best a decade of wavenumbers. This proves insufficient to distinguish between the various possible inertial ranges to be mentioned below. In the two-dimensional incompressible case, the inertial spectrum index has been determined at high-resolution with up to 2048×2048 grid points in a code using internal symmetries of the initial conditions (Brachet, Meneguzzi &

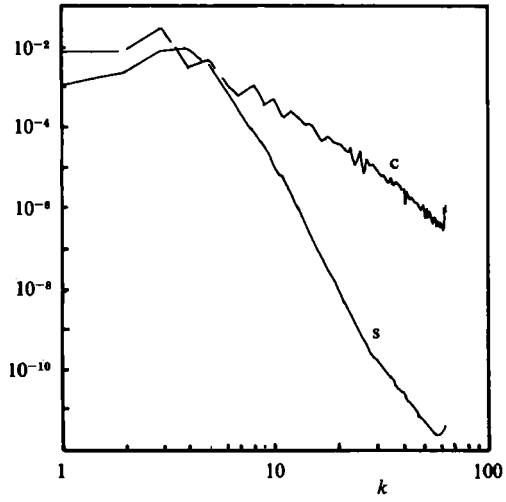

FIGURE 2. Energy spectrum decomposed into its solenoidal part (s) and compressible part (c) for the acoustic regime (run A).

Sulem 1985). It agrees with the $m = -3$ law proposed by Kraichnan (1967) on the basis of a statistical theory.

When, initially, the density fluctuations are stronger than Ma^2, even by a slight amount, the flow bifurcates towards a totally different regime. It rapidly transforms itself, with initial conditions mostly solenoidal, into the opposite quasi-potential flow in which the compressible modes represent more than 70 % of the kinetic energy and in which the density fluctuations become of the order of Ma. We show in figure 2 the energy spectrum decomposed into its solenoidal (s) and compressible (c) parts in this acoustic regime. The initial conditions are random with $Ma = 0.03$, and $Re = 50$. Furthermore, we define

$$\chi = \frac{E^{\mathrm{c}}}{E^{\mathrm{v}}} \tag{3.2}$$

as the ratio of the compressible energy E^{c} to the kinetic energy $E^{\mathrm{v}} = E^{\mathrm{c}} + E^{\mathrm{s}}$, where E^{s} is the solenoidal energy and where energies are integrated over the computational box. Here, we have initially $\chi = 0.07$; at time $t = 1.75$ at which the spectra are shown $\chi = 0.71$. Note that it takes a time $t = 0.6$ for a sound wave to travel across a distance L. The compressible modes are dominant at all scales, with an inertial exponent of the compressible spectrum close to 3.5. Such a spectrum has been proposed by L'vov & Mikhailov (1978*a*, *b*) on the basis of an equilibrium between the emission and absorption processes of sound, but for a slightly different context from the one modelled here.

Another model for compressible flows in the acoustic regime has been proposed by Zakharov & Sagdeev (1970); the argument is essentially that of dimensional analysis and leads in the two-dimensional case to a $k^{-11/7}$ inertial range, which we do not observe.

Two other possibilities should be mentioned. One concerns a phenomenological analysis, stating that shocks that lead individually to a k^{-2} spectrum do not have time to form (Moiseev *et al.* 1977), because of the effect of turbulent viscosity which dampens and considerably widens the shocks. Instead, a $k^{-\frac{3}{2}}$ spectrum should form, the argument being similar to that given by Kraichnan (1965) in the case of MHD

turbulence. The main point is that in the presence of waves (acoustic, or Alfvenic in the MHD case), energy transfer is considerably hampered and the efficiency of the cascade is diminished. Such a spectrum for two-dimensional MHD turbulence is in the simpler cases compatible with recent numerical simulations (Pouquet, Sulem & Meneguzzi 1986). But it should be noted that, in the MHD case, a supplementary geometrical effect comes into play. Indeed, the wave propagation is well ordered, taking place along the magnetic field lines of the large-scale (or uniform) field. However, in the acoustic case, we are not aware of such a geometrical effect. This may explain the different behaviour we find in the numerical simulations of the two cases, acoustic and Alfvenic.

Finally, we should mention a theoretical determination (Moiseev *et al.* 1981) of the correction to a Kolmogorov spectrum due to weak compressibility. The analysis, using diagrammatic techniques and also self-similarity arguments is done in the three-dimensional case; the authors find a correction of order M^2 to the celebrated $-\frac{5}{3}$ law. As mentioned before, the two-dimensional inertial-range index is more likely to be equal to -3 in the incompressible regime, unless coherent structures play a dominant role. One may thus expect a $-3+O(M^2)$ for the acoustic regime in two dimensions, which would be consistent with our results. Such an analysis requires that the sink of energy in the inertial range due to weak compressibility induces as well an enstrophy dissipation. However, note that in the two-dimensional incompressible case, it is known that enstrophy transfer is markedly nonlocal (i.e. involves widely separated scales) in contrast to the three-dimensional case, and thus the sink of enstrophy may appear at a higher order in Mach number.

Such weak acoustic turbulence is characterized by flow structures that are displayed in figure 3. The thin layers correspond to weak shocks, with negligible entropy jumps, and this kind of flow does not actually require a treatment of the energy equation. The density contours of figure 3 are shown at $t = 1.75$. A typical jump in the density is 0.1 (normalized value). These weak shocks will be as thin as the resolution permits, i.e. a few grid points across. This condition is fulfilled, as stated before, by a proper choice of the Reynolds number; in particular, we verify that there is little or no rise in the spectra in the vicinity of the maximum wavenumber of the computation.

We are not able to say what determines the longitudinal extent of these shocks. Do initial conditions prevail, with the average length of the density structures that at the initial time? There is some evidence for this, but we also observe merging of these shocks with time, with the formation of slightly curved density filaments, like the one visible in the centre of figure 3. A study of long-time behaviour of this and other flows may be undertaken, making use of various techniques ranging from a modified viscosity to a more sophisticated parametrization of the small scales. This point will be discussed further in §6.

Finally, we wish to stress that in all the calculations we have performed at low Mach number, the inertial spectra are clearly steeper than k^{-2}. This latter value has been predicted by several authors (Kadomtsev & Petviashvili 1973; Elsasser & Schamel 1976) in the case of weak shocks for either one-dimensional or two-dimensional turbulence. This is also the spectrum for the turbulence described by the Burgers' equation, and corresponds to the formation of quasi-discontinuities. In fact, Tatsumi & Tokunaga (1974) showed using multiple-scale analysis that in the one-dimensional case for low-amplitude fields, large scales and long times, the flow evolves towards that described by Burgers' equation. The extension of their analysis to the stationary two-dimensional case can be done (Tokunaga & Tatsumi 1975),

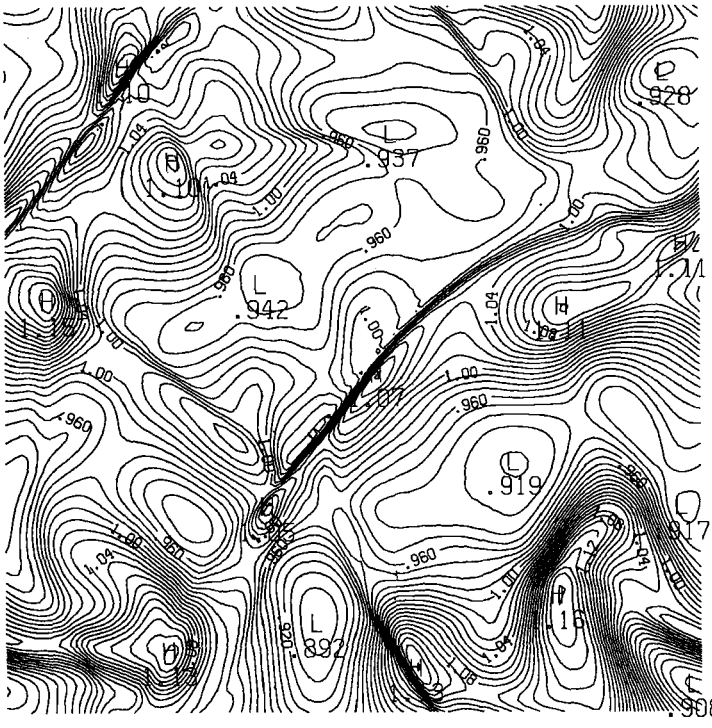

FIGURE 3. Density field for the acoustic regime (run A) at $t = 1.75$.

arguing that elongated structures necessarily form (since a shock is likely to be of finite extent and small width) and that they are quasi one-dimensional and isolated in space. Thus, this will again eventually lead to a k^{-2} Burgers-like spectrum.

The reasons why we do not find such shallow spectra may be twofold. On the one hand, our codes still lack sufficient resolution to be in the conditions described in the theoretical works. In particular, the inertial range and the dissipative range are not markedly separated. Moreover, the inertial range may be contaminated by power-law prefactors preceding the viscous range which arise when the structure of the complex-plane singularities of the flow may not be simple poles any more. Indeed, it is found both analytically (using a dominant balance analysis) and numerically that the leading singularities arising in a one-dimensional model of the compressible case are more complicated, and lead to crest-like irregularities in the energy spectra (T. Passot 1986, paper in preparation). On the other hand, the aforementioned theoretical approaches do not take into account the statistical interaction of the numerous weak shocks present in our simulations, as can be seen in figure 3. As in the two-dimensional incompressible case, such interactions may lead to a different spectrum from that constructed from simple analytical solutions; in that case vorticity jumps leading to a k^{-4} spectrum (Saffman 1971). Finally, we note that a Burgers'-like turbulence may arise only for long times, as predicted and observed numerically from Lighthill's (1956) equations by Tokunaga (1976).

In order to check this point we have performed a one-dimensional numerical simulation of a compressible gas using the complete equations of a perfect gas. Starting with a Mach number of 0.5, we observe two distinct phases in the evolution of the flow. At first, shocks form that are separated by rarefaction waves, i.e. by

regions in which the density varies substantially. Corresponding velocity spectra are rather steep, with a slope of the order of -3. For late times when a substantial amount of the kinetic energy has disappeared into heat, the flow is indeed made up of triangular N waves (Lighthill 1956) and density structures are simple plateaux of various heights. The velocity spectrum has now become shallower, and its slope is close to -2, as expected for a flow only made up of jumps. In the former case (early time), however, the rarefaction waves provide a smoothing effect, since the density gradients in them are less sharp than in shocks; hence a steeper spectrum. To observe a similar effect in the two-dimensional case seems unnecessarily costly. One possibility, which will be further discussed in §6, is to artificially enhance the Reynolds number by using dissipation functional forms different from those of the original equations. This work is now in progress and will be reported elsewhere (Passot & Pouquet 1987).

4. The strong Mach-number regime

We now examine the case of an initially strongly compressible flow, with a r.m.s. value of Mach number ranging from 0.3 to 2. The various theoretical and phenomenological analyses quoted in §3 do not apply to this regime, where density fluctuations are of order one and compressible effects can no longer be considered a perturbation on a vortical flow. However, as we shall see in §5, the acoustical character of the flow is still felt in the large scales.

In all the cases we ran, with random initial conditions in which the ratio of the compressible to the kinetic energy χ varies between 0 and 0.6, we systematically observe that small scales are dominated by shocks and large scales by vortices. We display in figure 4 the contours of (*a*) the divergence of the velocity field and (*b*) the vorticity at time $t = 1.375$. For this run at $Ma = 1.65$, it takes a sound wave a time $t = 10$ to cross the box of size $L = 2\pi$; the initial Reynolds number is $Re = 115$ and $\chi = E^{\mathrm{c}}/E^{\mathrm{v}} = 0.12$ (resolution of 256×256). Several shocks are seen in the divergence plot, with maxima of the divergence around -5. Their width is due to viscous effects, and these widths are in a sense the smallest dynamical scales actually resolved by the computation. On the vorticity plot, we see that vortices are most intense in the vicinity of such shocks, with the same longitudinal extent but with a greater width. In that run, shocks form in pairs because of their strength. Indeed, with an r.m.s. Mach number of 2, local Mach numbers up to 3.6 can be observed in individual shocks in which the density jump approaches its limit value of 6 (for $\gamma = 1.4$). In figure 5, we display an oblique profile across a double shock at a later time than figure 4, for the same run. The density jump here is close to 5 and the temperature jump close to 2. In such shocks, entropy is produced, along with a strong local heating. This computation is particularly well resolved, as can be seen from the profiles in figure 5, where all the computational points are displayed. The strong density gradients of both shocks occur on 8–10 grid points. This run could be performed at a higher Reynolds number, reducing this shock width to half its present value, but oscillations will then appear and be particularly visible in the divergence and vorticity contours that enhance small-scale behaviour.

The time sequence of the evolution of the flow may be as follows. Starting with a quasi-incompressible distribution of eddies concentrated in the large scales ($k_0 \sim 2$), shocks appear in a time of order unity in pairs whose elements then move farther apart as time proceeds. This phase is followed by interactions between the various shocks that are of two different types. In a collision, the shocks may either ignore

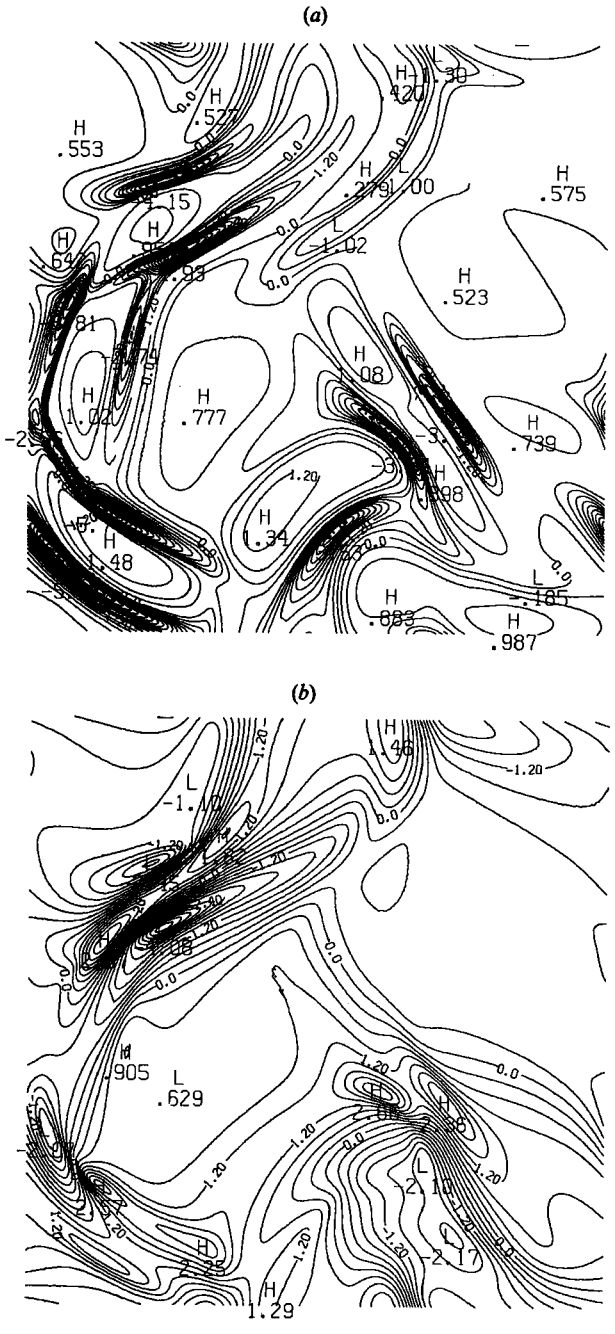

FIGURE 4. Divergence (a) and curl (b) of the velocity field for a flow with initial Reynolds number of 115 and r.m.s. Mach number of 1.65 (run B) at $t = 1.375$.

each other and continue their path with a slightly different velocity, or they can coalesce. What distinguishes the two behaviours is a combination of kinetics and geometry. The preceding process can repeat itself, with successive shock formation, collision and possible coalescence. We observe in general that the number of shocks in the box tends to diminish with time, with the formation of structures that are

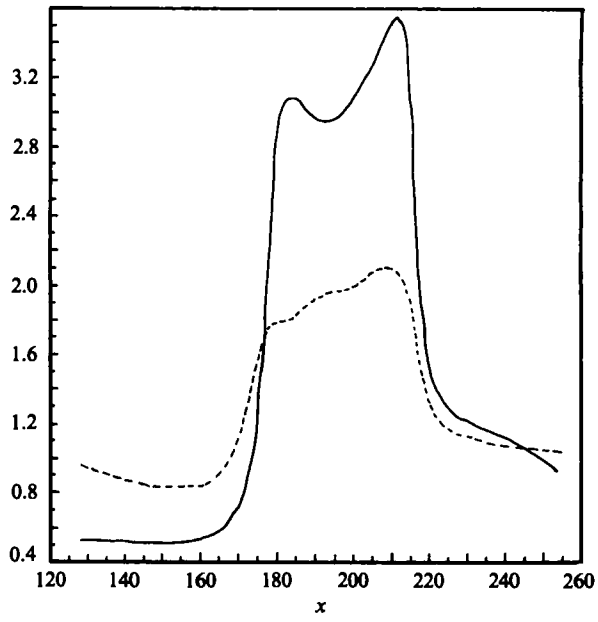

FIGURE 5. Oblique profile of the density (solid line) and temperature (dotted line) in a double shock for run B.

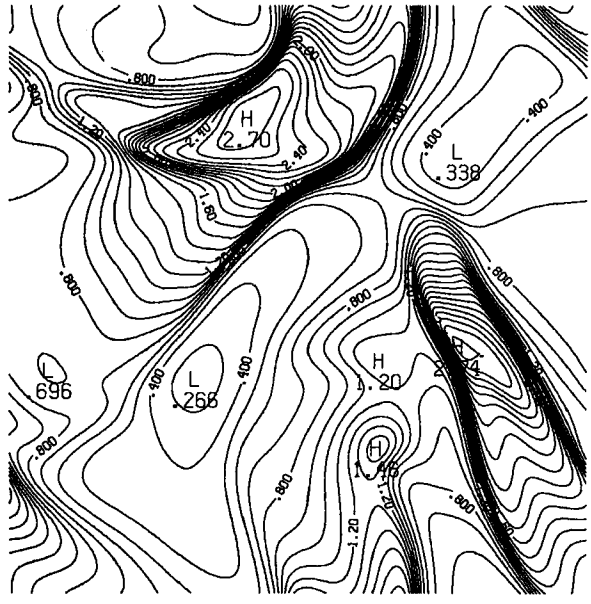

FIGURE 6. Density contours at a later time ($t = 3.25$) for run B.

quasi-one-dimensional and somewhat elongated, as displayed in figure 6, which gives the density contours at $t = 3.25$ for the same run as in figures 4 and 5.

Let us finally note that the interaction between a shock and a vortex can be of several types. On the one hand, vortices are flattened by shocks, with the formation of shear layers; this is particularly visible in the lower-Reynolds-number runs. On

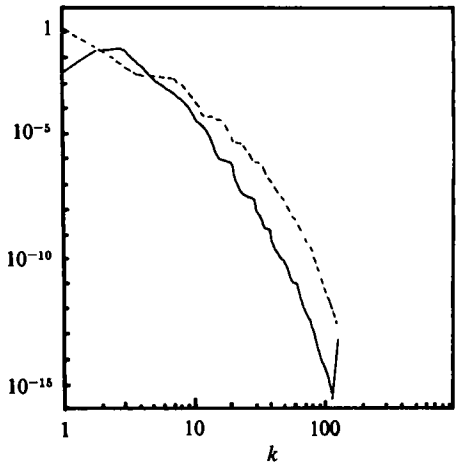

FIGURE 7. Energy spectrum, with solenoidal (solid line) and compressible (dotted line) components, the latter being dominant in the small scales (run B).

the other hand, vortices are formed behind a shock, with a scale larger than that of the width of the shocks. A third possibility, which may be the dominant effect in highly turbulent flows, will be suggested below.

The domination by shocks in the small scales of the flow is particularly evident on the energy spectra shown in figure 7 for the same run as in the preceding figures. The longitudinal modes are overwhelming in the small scales, by three orders of magnitude. Similar results hold for other runs in the strong-Mach-number regime, and this is also the case for the barotropic case (Léorat *et al.* 1983). In the large scales, vortices can prevail over compressive modes, roughly by a factor five at $k = 3$ in run B (see table 2).

The spectra of the velocity components u_x and u_y in the x- and y-directions are indistinguishable at all scales (not shown). This is because, although individual shocks are highly anisotropic with a width negligible compared to their length, the number of shocks in the box is sufficient to ensure isotropy. On the other hand, at later times when most shocks have disappeared, x- and y-velocity spectra begin to show some discrepancy, up to a factor three. A remarkable feature is that the temperature spectrum, for large enough Reynolds numbers, is in almost exact equipartition with the velocity (u_x and u_y) spectra.

Concerning the small scales, the result presented here is in contradiction with a prediction of Kraichnan (1953) based on general arguments of statistical equilibrium. In the small scales, the typical interaction time between shocks and vortices is small enough that equipartition between the various modes should be reached. We find no clear variation of the ratio $\chi_{ss} = E^c_{ss}/E^v_{ss}$ (ss referring to small-scale quantities) with either Reynolds number or Mach number. The transition between the weakly compressible case, in which the opposite situation occurs with predominance of the vortices at all scales, is sharp, and occurs at a Mach number of 0.3. The lack of equipartition at high Mach number could be a dimensional effect: the conservation of enstrophy in the incompressible case may play a role. We are presently writing a code for the three-dimensional case which will run on a more powerful machine to check this point. Preliminary results (Passot 1987) at a Reynolds number of 230 and a Mach number of 2.2 on a $128 \times 128 \times 128$ grid indicate that equipartition may not

be reached in three dimensions either. Such results may be because the Reynolds numbers achieved in our computations are not sufficient to let efficient interaction between shocks and vortices take place. We must stress the fact that the compressible problem has proven to be harder to properly resolve than previous studies we performed in the incompressible Navier–Stokes or MHD case in the sense that, for a given grid, the reasonably attainable Reynolds numbers are somewhat lower here. This may be linked to the fact that two-dimensional hydrodynamic flows are known to be smooth for all times (Wolibner 1933) and two-dimensional MHD flows are also thought to be smooth for long times (Frisch *et al.* 1983), the flattening of current sheets at neutral X-points presumably occurring only exponentially with time (Sulem *et al.* 1985). On the other hand, in the compressible case, shocks form in a finite time. The investigation of the small-scale structure of the flow requires careful numerical integration. One way to enhance the Reynolds number is to modify the small scales, and several possibilities have been tried in different contexts. This point is discussed more at length in §6.

But clearly this will not help to resolve the problem at hand. However, the brief description of another case we ran may shed some light on the evolution of high-Reynolds-number compressible flows. We have performed a run, with the 256×256 grid, in which initially $Re = 300$, $Ma = 1.1$ and $\chi = 0.58$ (run C). The overall temporal evolution of the flow is similar to what has been described before. The higher Reynolds number simulated here is rendered possible by the fact that the Mach number is smaller than for run B: shock formation is less efficient and less viscosity is needed to smooth out the flow. The novel feature of this run appears in the display of the production term of vorticity ω. We write omitting dissipation terms:

$$\frac{\mathrm{D}\omega}{\mathrm{D}t} = P_\omega - \omega(\operatorname{div} u) \tag{4.1}$$

where D is the Lagrangian derivative and the production term of vorticity P_ω is given by

$$P_\omega = -\frac{1}{\rho^2}\nabla p \times \nabla \rho = (\nabla T \times \nabla S)\rho, \tag{4.2}$$

with p the pressure, T the temperature and S the entropy. Note that this term is zero in the barotropic case ($p = \rho^\alpha$). This increase in the vorticity happens at the expense of the internal energy, as (4.2) shows; we checked that on the energy spectra, when such vortices appear, the solenoidal spectrum gains in power whereas the compressible spectrum remains the same.

We show in figure 8 the contour lines of P_ω for run C at $t = 3.6$. At later times, the overall vorticity production will be of the same nature but less intense, because of the decrease over time of the Reynolds number, and the P-spots will be situated elsewhere. The striking feature of figure 8 is the spatial intermittency of P_ω, with well-defined finite-extent eddies of a size intermediate between the length and the width of the shock. The intensity of P_ω at the time shown in figure 8 goes up to 100, whereas typical numbers for either ∇p or $\nabla \rho$ are of the order of 10. Since no cavitation is observed at such locations, the effect is mostly geometrical in nature, namely with the gradients of pressure and density (or temperature and entropy) almost orthogonal.

These P-eddies are localized in zones where two strong shocks interact. Figure 9 shows the full flow for run C at the same time, and a blow-up of the upper-left collision is given in figure 10 at $t = 4.0$. In the matching region of the two quasi-linear shocks,

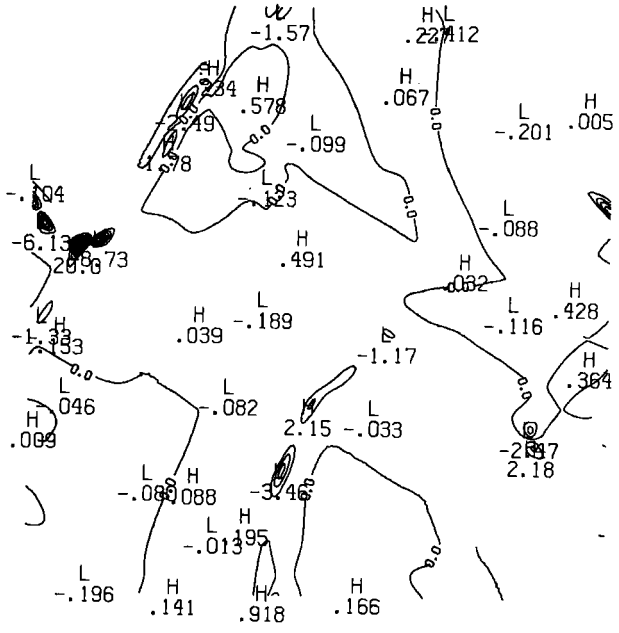

FIGURE 8. Contour lines of vorticity production term defined in (4.2) for run C at $t = 3.6$. Note its strong spatial intermittency.

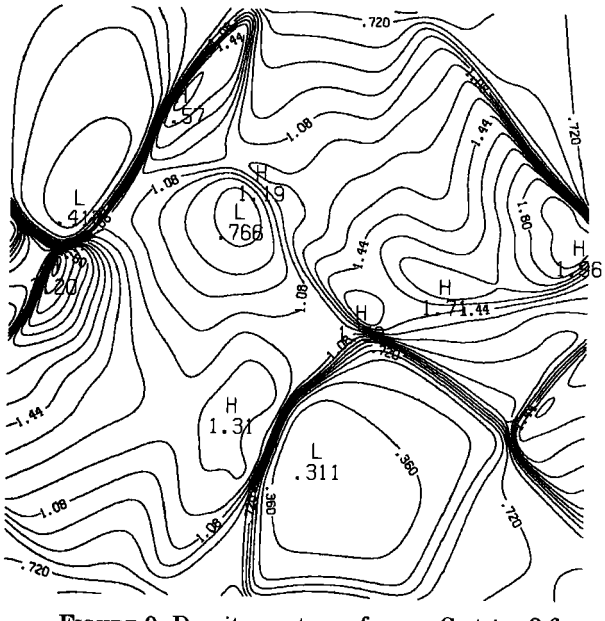

FIGURE 9. Density contours for run C at $t = 3.6$.

the size of which is determined mostly by viscosity, two vortices of opposite polarity form. As time proceeds, their widths remain approximately the same, and their lengths augment along the two initial shocks through line stretching. Because of their rather small size, dissipative effects take place in a time less than one and these structures finally disappear, being replaced by similar pairs of vortices where other

shocks collide. The intensity of these vortices dominates the surrounding background flow and is evident in the spectra. Figure 11 shows the energy spectra, decomposed as usual into solenoidal and compressible parts, for run C at time $t = 4$. One can no longer speak, in such a case, of an inertial range with a power law. The visible crests on the solenoidal spectrum are at a scale that corresponds to the observed vorticity pairs, and form at larger wavenumbers at later times. In time, such pairs are created and destroyed, with sizes that decrease since shocks become weaker. The spectra have thus a complex temporal evolution. However, on average, the solenoidal spectrum may be brought close to its equipartition value with the compressible one.

There is a simple physical reason for the production of vorticity in the narrow zone delineated by the shock collision. We shall first recall the analysis of shock collisions, following Landau & Lifshitz (1959). In figure 12(*a*), we sketch the well-known geometry of an oblique shock. The velocity component $V_\perp$ orthogonal to the shock is shown with a dotted line, and the tangential component $V_\parallel$ with a wavy line. Shock conditions are such that $V_\perp$ is supersonic behind the shock and subsonic in front of it. On the other hand $V_\parallel$ – which does not undergo a jump – can be supersonic, in which case the shock may be oriented as indicated by the double arrow in the sketch. This representation of a shock specifies in fact the direction of propagation of a sonic disturbance, in the same direction as the tangential post-shock velocity. This type of diagram is useful in classifying possible configurations in multiple shock collisions. When two strong shocks meet, a likely configuration is that shown in figure 12(*b*) in which, in region IV, there must exist in general a tangential discontinuity in the velocity, indicated by the broken line; note that conditions for a ternary collision are more stringent and thus it is easier to observe the 4-collision shown in figure 12(*b*). It is this shear that is very likely at the source of the vorticity in our numerical simulation; the observed configuration of shock collisions is indeed that of figure 12(*b*), with vortices of the width of the shear layer, governed as already noted by viscosity. The reason for the opposite polarities of the vortices across the contact discontinuity is clear when one considers the geometry of the flow in the cone of shear turbulence occurring at the shock collision. In that region, as shown on figure 12(*c*), the entropy gradient ∇S and the temperature gradient ∇T across the two shocks are such that their vector product changes sign at the contact discontinuity (see (4.2)). In that light, a high-resolution study of Kelvin–Helmholtz instability is useful. A careful analysis of the data using an image processor with raster technique shows clearly, on the density field, the existence of turbulence in this region, whereas in the three other domains in the vicinity of the collision, the density varies more smoothly. We should, however, note at this point that textbook shocks with constant density on each side of the jump are not likely to be found in our computation. Indeed, shocks are not isolated, but interact with a multiplicity of structures, rendering the matching of density zones complex enough that rarefaction waves are found everywhere. As already noted, this is probably at the source of the steep energy spectra that we observe. Furthermore, the data displayed and analysed here are for times of the order of a few eddy turnover times. For larger times, we expect that these rarefaction waves will disappear, leading to a simpler aspect of the flow, with a few elongated shocks with zones of quasi-constant density between them. The effective Reynolds number of this shear turbulence, which must be computed on the limited size of the region where the discontinuity prevails, is substantially lower than the Reynolds number based on the large scale of the flow. This may be the reason why the solenoidal part of the energy spectrum is extremely steep, with a relatively small effective dissipation wavenumber.

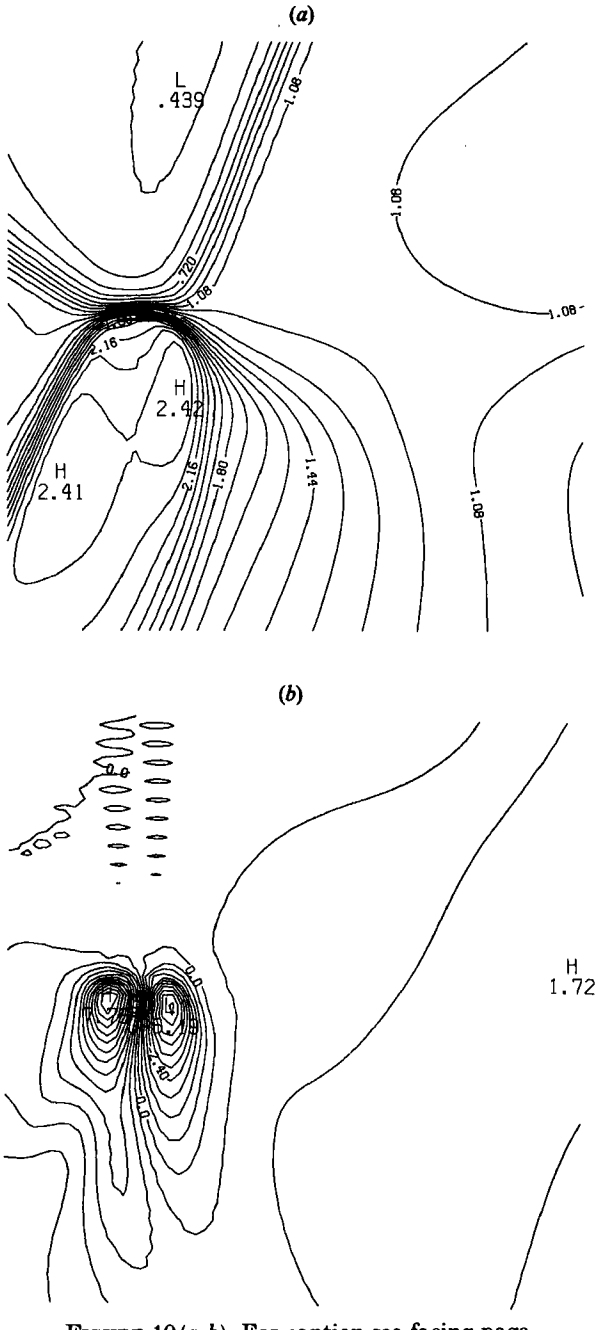

FIGURE 10(*a*,*b*). For caption see facing page.

We now return to the question of equipartition between vortex and shock in the small scales. At high Reynolds numbers, one possible scenario is that vortices are formed in strong colliding shocks at an intermediate scale and with a sufficient intensity to be able to survive on times of order one. Through mixing of such vortices, and nonlinear cascading towards small scales, it is possible that equipartition may

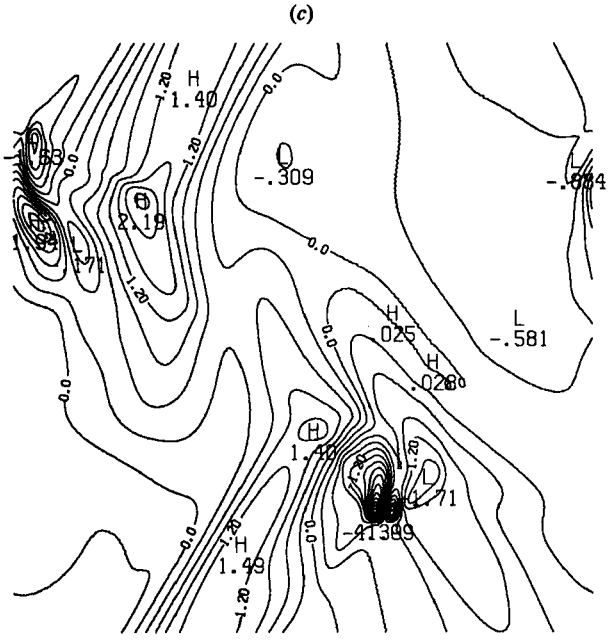

FIGURE 10. (*a*) Blow-up of figure 9 (upper-left collision); (*b*) vorticity in the same region, $t = 4.0$; (*c*) vorticity at a later time maximum, $t = 4.8$.

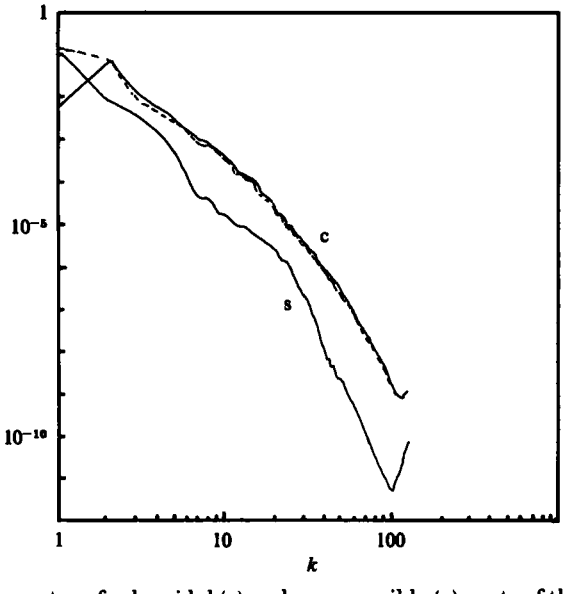

FIGURE 11. Energy spectra of solenoidal (s) and compressible (c) parts of the velocity at time $t = 4.0$ for run C. Notice the crests in the solenoidal spectrum, at an intermediate wavenumber corresponding to the production of vortices shown in figure 10(*b*).

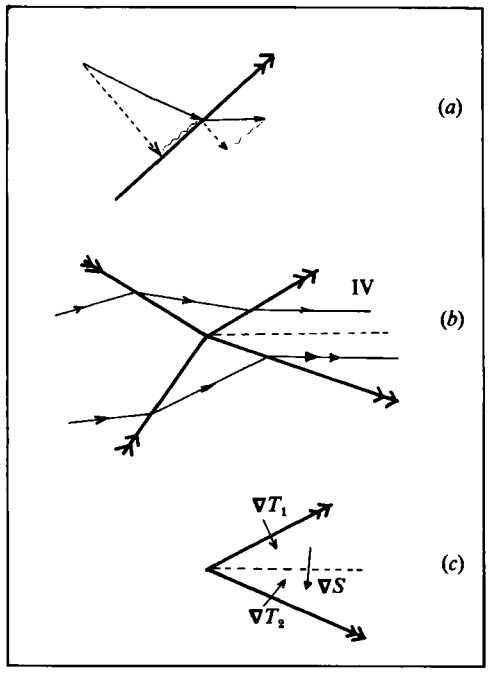

FIGURE 12. Sketches of (*a*) an oblique shock; (*b*) the collision of two shocks: the large arrows indicate the orientation of the shocks (see text); the broken line corresponds to a tangential discontinuity; (*c*) the temperature and entropy gradients at the origin of bipolar vortices (see equation (4.2)).

be finally reached. This problem seems particularly sensitive to numerical resolution, since these vortices form in the advent of shock collisions which occur after shocks have formed. In other words, the production of vorticity through shear occurs when the calculation is already well advanced, i.e. when the Reynolds number has already decreased somewhat. Again, a parametrization scheme that allows one to slow down the dissipation of mechanical energy may prove useful in this instance (see §6).

5. Large-scale long-time behaviour of a supersonic flow

In a two-dimensional incompressible flow, energy is barely dissipated, because of the constraint on the nonlinear terms of the enstrophy conservation (in the inviscid case). In a compressible flow, both the shocks and the acoustic waves contribute sizeably to the energy dissipation. In the absence of an external source, therefore, a supersonic flow cannot remain so forever and the question arises as to whether the energy depletion renders the flow eventually incompressible or whether the Mach number remains substantial for long periods of time.

Several energetic quantities can be defined. The mechanical energy E_{mech} is computed by subtracting from the total constant energy E the internal energy associated with the mean temperature. A more correct computation taking into account the instantaneous dissipation would be too costly since it requires evaluating several more FFTs. It was verified on low-resolution runs (64×64) that both formulations agree to within 9 %. The compressible E^{c} and solenoidal E^{s} energies are the sums over the computation box of their respective Fourier components, with $E^{\mathrm{v}} = E^{\mathrm{c}} + E^{\mathrm{s}}$ being the kinetic energy. The internal energy e is such that the total

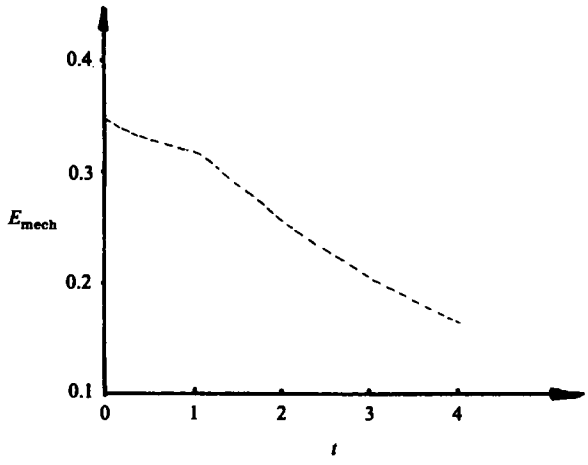

FIGURE 13. Temporal evolution of the mechanical energy for run C. Increased dissipation sets in at the time of formation of the shocks.

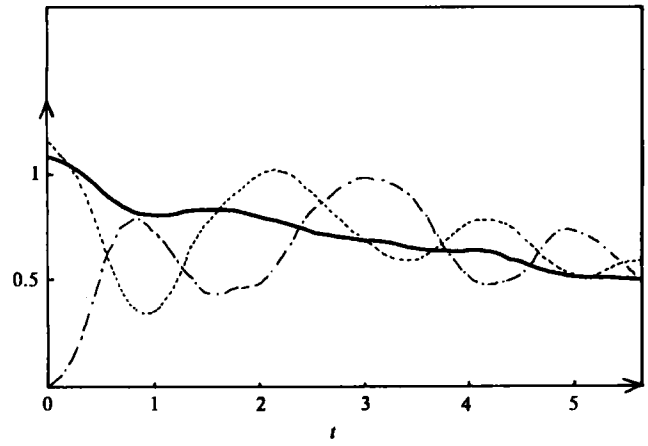

FIGURE 14. Temporal evolution for run C of the r.m.s. Mach number (solid line), the ratio χ of the compressible to the kinetic energy (dot-dashed line) and the ratio of the internal to the mechanical energy (mixed line). Note the plateaux in the Mach number curve, indicating periods of replenishing the reservoir of compressible energy.

energy is $E = \rho(e + E^{\text{v}})$. Depletion from the kinetic energy source fills the internal energy and augments the temperature, and vice versa.

We show in figure 13 the time evolution of the mechanical energy for run C. The clear break in the curve occurring at $t = 1$ corresponds to the time of shock formation, at which dissipation of the mechanical energy into heat is enhanced. However, if we now plot the temporal evolution of the r.m.s. Mach number, a new phenomenon appears (figure 14): the decrease in the Mach number (solid line) is interrupted by several successive plateaux (see also Passot & Pouquet 1986). Such plateaux are associated with quiescent periods in the flow when the kinetic-energy reservoir is being replenished. Shocks can then again form and dissipate energy efficiently, and so on, thus provoking a dualistic temporal behaviour of the flow evolution which appears periodic. Indeed, when we plot (in figure 14) against time the ratios (dotted line) $\chi = E^{\text{c}}/E^{\text{v}}$ and (dot-dashed line) $r = e/E_{\text{mech}}$ (which can both vary between 0

and 1), we observe quasi-linear oscillations. Although χ and r are independent, they are found to evolve almost in phase opposition (Passot & Pouquet 1986).

This type of oscillatory behaviour has been predicted (Tatsumi & Tokunaga 1974) for flows that are simpler than the one studied here. Those authors looked at the one-dimensional case in the limit of small Mach numbers, using for that case the equations due to Lighthill (1956). They show analytically and numerically that the spectral density $r(k)$ at scale k^{-1} oscillates linearly in time with a frequency proportional to k. Thus the integrated ratio r, which is dominated by the large-scale components of the spectrum, undergoes an oscillation in which the dominant frequency is that linked to the integral scale l_0. Other scales give small contributions because of the fast decreasing spectrum towards large wavenumbers. At high Reynolds numbers, more modes intervene and this can explain the visible departure from a pure sinusoidal behaviour in figure 14. This type of oscillatory behaviour is reminiscent of the acoustic exchanges that would be dominant at small Mach numbers. The fact that we still observe them in our simulations is linked to the persistence of the large-scale-containing eddies of a turbulent flow, even in the compressible case. Large-scale oscillations have also been reported for two-dimensional incompressible MHD calculations (Pouquet *et al.* 1987) and in three-dimensional stratified flows (M. Lesieur, private communication).

For a large variety of Mach numbers and integral scales l_0, we find that the period of oscillation of the energy ratios χ and r is linearly related to the characteristic time of propagation of a sound wave over a distance l_0. More precisely, we can in fact relate these oscillations to the interactions between the various waves propagating in the flow. The resolution reasonably achieved on a CRAY-1 computer on a uniform grid for the compressible two-dimensional problem is 256×256 points. Non-uniform grids would allow us to resolve finer scales of the flow, but appear difficult to implement for the type of configuration treated in this paper where flows are assumed homogeneous but nevertheless develop intricate structures evolving in time. With such resolutions, the natural choice in the initial conditions is one for which the width of individual eddies is approximately equal to their mutual separation. Thus, the intrinsic eddy turnover time and the acoustic propagation time are roughly the same. If one now considers several sets of wavetrains whose separation is much greater than their width, we should observe in the time evolution of the energy ratio χ and r a succession of nonlinear pulses at times at which the wave packets interact, followed by quiescent periods. We performed such a computation in the one-dimensional case and indeed found that it was so.

The striking feature in the time evolution of the Mach number consists in the fact that it denotes a collective behaviour, in the sense that coherent effects play a role in slowing down its decrease. It also indicates that the kinetic energy can persist in significant amounts for times long compared to the time of formation of individual shocks, because such dissipation does not occur continuously but in bursts. In fact, there are moments at which the flow pumps kinetic energy from the internal energy in order to form subsequent shock waves. This phenomenon may be enhanced by periodic boundary conditions, but we have verified that it persists in one-dimensional high-resolution runs with initial conditions restricted to a small portion at the centre of the box.

Long-time ($\omega \to 0$) large-scale ($k \to 0$) behaviour properties of a turbulent flow are amenable to a renormalization group analysis (Forster, Nelson & Stephen 1977; Sulem, Fournier & Pouquet 1979). However, in the fully compressible case, technical difficulties arise owing to the high degree of nonlinearity appearing in the equations.

The problems treated with such diagrammatic techniques have been in the acoustic regime, looking in particular to corrections to the Kolmogorov $-\frac{5}{3}$ law. In view of the oscillatory behaviour we obtain here, one cannot discard the hypothesis that the renormalization procedure may lead to the appearance of new terms in the equations (in the limit $\omega \to 0$, $k \to 0$) of the vertex type or of the eddy-viscosity type, possibly complex as has been found by Pelletier (1980) in the problem of Langmuir waves.

6. Conclusion

We have investigated, in this paper, two-dimensional homogeneous flows in the subsonic and supersonic regimes, using direct numerical simulations. In the subsonic case, and for density fluctuations of the order of the squared Mach number, the flow retains its incompressible character at all scales, the acoustic level remaining low. In the supersonic case, the opposite occurs, with a strong domination of longitudinal modes in particular in the small scales of the flow. The transition between the two regimes occurs at an r.m.s. Mach number of 0.3. It is conceivably because of the quadrupole nature of the emission of sound that the subsonic regime persists to rather high values of the Mach number. This result corroborates the fact that the Lighthill (1955) formula for the change in the dissipation rate of energy is known to hold up to similar values of Ma.

The other striking feature of our results is that shear turbulence may be produced from shocks, as conjectured by various authors (see, for example, Lighthill 1955). Such a production occurs locally, in particular in the narrow region downstream of the collision of two supersonic shocks, with a clear vortex-pair production of an intensity significant enough to be clearly visible on the energy spectra. This effect is also felt in the way energy is exchanged between the available modes (solenoidal, longitudinal, internal) and in the fact that the Mach number does not necessarily decrease monotonically with time.

Finally, the anisotropy of individual shocks – which are of finite extent and as thin as viscosity will allow – is compensated by the presence of various other shocks in the flow, of random orientation, yielding isotropic velocity spectra. However, the strong local anisotropy in regions of strong density gradients has important consequences when self-gravity is switched on, giving rise to elongated structures in the form of filaments (J. Léorat, T. Passot & A. Pouquet, paper in preparation).

In order to pursue this type of work to apply it to astrophysical problems such as the role of turbulence in star formation, one needs to investigate the behaviour of flows for long times and at high Reynolds numbers.

Few theoretical models for a fully turbulent and compressible flow have been developed. For example, two-point closures which have been widely used for incompressible turbulence (Pouquet 1984) are difficult to implement in the compressible case, because of the high degree of nonlinearity in the original equations. However, Weiss (1979) has written such a closure scheme via modelling of the pressure term which renders the equations quadratically nonlinear, and thus simpler to handle algebraically. A numerical integration of those equations enabled Weiss to show that, in two as well as in three dimensions, the flow remains quasi-incompressible for all times. Our results confirm the validity of the model, in two dimensions at least, up to an r.m.s. Mach number of 0.3. Such models may thus be very useful in a variety of situations from the re-entry problem of space vehicles, to subsonic turbulence in molecular clouds. In particular, they are easier to handle both analytically and numerically than the primitive equations, and provide in a simple way time-

dependent and spectrally dependent expressions of transport coefficients such as eddy viscosities. We are in the process of evaluating these coefficients and implementing them in a large-scale simulation as a possible way to parametrize the small scales of the flow, as already done in the incompressible case (Chollet & Lesieur 1981; Lesieur 1984).

Numerical simulations prove to be an experimental tool complementary to those available in the laboratory. It permits one to investigate a range of parameters of importance, for example in astrophysical problems of high fluctuating Mach number, of high magnetic Reynolds number, to name two, which are not accessible in the laboratory. Moreover, it gives a direct evaluation of derivative fields such as the vorticity and, in MHD, the current, hence important dynamical quantities such as the helicity (Moiseev *et al.* 1983) can be computed, whereas such measurements in the laboratory are difficult, both with hot-wire anemometry or laser-Doppler velocimetry. On the other hand, the clear drawback of the numerical approach taken as an experimental tool is its limitation in resolution, i.e. in reasonably and reliably attainable Reynolds numbers.

One possible way to simulate highly turbulent flows is to couple together a numerical integration of the large scales and a parametrization of the small scales. This approach is followed in the treatment of compressible inhomogeneous flows by Ha Minh & Vandromme (1986) by extending existing k–ϵ models. As mentioned before, in the homogeneous case, one can make use of analytical expressions for transport coefficients.

Another approach is to use some form of artificial viscosity, assuming that the flow is inviscid in the whole domain except in shocks and contact discontinuities. Without resorting to this method, it is customary with spectral codes to use hyperviscosities, i.e. a modified power of the Laplacian, for example a bi-Laplacian. Such a term concentrates the dissipation in a narrow range of wavenumbers near the cutoff k_{max}, thus leaving more room for the inertial range. However, hyperviscosity seems less satisfactory in the compressible case, in particular because it creates spurious oscillations near the shocks and leads to the appearance of zones in which energy is created (at the expense of the internal-energy reservoir) instead of being dissipated. This defect can be remedied, and we are presently working on that problem, in particular to investigate the oscillatory behaviour of the large scales (Passot & Pouquet 1987).

We have used the FFT algorithm written by C. Temperton, and the graphical software of NCAR. Computations have been performed on the CRAY-1 of the Centre de Calcul Vectoriel pour la Recherche under contracts 1630 and 3674. We are thankful to J. Léorat for useful discussions. This work received financial support from the CNRS through the RCP 'Fluides astrophysiques en régime supersonique' under contract number 080702, and the ATP 'Dynamique des fluides astrophysiques et géophysiques' under contract number 1227.

REFERENCES

Abarbanel, S., Gottlieb, D. & Tadmor, E. 1985 Spectral methods for discontinuous problems. ICASE *Rep.* 85-38.

Brachet, M. E., Meneguzzi, M. & Sulem, P.-L. 1985 In *Macroscopic Modelling of Turbulent Flows* (ed. U. Frisch, J. B. Keller, G. C. Papanicolaou & O. Pironneau). Lecture Notes in Physics, vol. 230, p. 347. Springer.

BRACHET, M. E. & SULEM, P.-L. 1985 *Prog. Astronaut. Aero.* **100**, 100.

CHACON, T. & PIRONNEAU, O. 1986 *DRET-ONERA Colloquium, Poitiers, Ecole Nationale Supérieure de Mécanique et Aérotechnique*, pp. 27–38.

CHOLLET, J. P. & LESIEUR, M. 1981 *J. Atmos. Sci.* **38**, 2747.

CRIGHTON, D. G. 1975 *Prog. Aerospace Sci.* **16**, 31.

ELSÄSSER, K. & SCHAMEL, H. 1976 *Z. Phys.* **B 23**, 89.

FARGE, M. & SADOURNY, R. 1987 Inertia-gravity wave effects on a decaying two-dimensional turbulence in rotation. *J. Fluid Mech.* (submitted).

FEIEREISEN, W. J., REYNOLDS, W. C. & FERZIGER, J. H. 1981 Numerical simulation of a compressible, homogeneous turbulent shear flow. *Rep.* TF-13, Thesis, Stanford University.

FORSTER, D., NELSON, D. R. & STEPHEN, M. J. 1977 *Phys. Rev.* A **16**, 732.

FRISCH, U., POUQUET, A., SULEM, P. L. & MENEGUZZI, M. 1983 *J. Méc. Théor. Appl., numéro spécial*, p. 191.

GAFFET, B. 1985 On generalized vorticity-conservation laws. *J. Fluid Mech.* **156**, 141.

GOTTLIEB, D. & ORSZAG, S. A. 1977 *Numerical Analysis of Spectral Methods.* Philadelphia: SIAM.

HA MINH, H. & VANDROMME, D. D. 1986 *DRET-ONERA Colloquium, Poitiers, Ecole Nationale Supérieure de Mécanique et Aérotechnique.*

KADOMTSEV, B. B. & PETVIASHVILI, V. I. 1973 *Sov. Phys. Dokl.* **18**, 115.

KRAICHNAN, R. H. 1953 *J. Acoust. Soc. Am.* **25**, 1096.

KRAICHNAN, R. H. 1965 *Phys. Fluids* **8**, 1385.

KRAICHNAN, R. H. 1967 *Phys. Fluids* **10**, 1417.

LANDAU, L. D. & LIFSHITZ, E. M. 1959 *Fluid Mechanics.* Pergamon.

LARSON, R. B. 1981 *Mon. Not. R. Astron. Soc.* **194**, 809.

LÉORAT, J. & POUQUET, A. 1986 *DRET-ONERA, Colloquium, Poitiers Ecole Nationale Supérieure de Mécanique et Aérotechnique*, pp. 101–110.

LÉORAT, J., POUQUET, A. & POYET, J.-P. 1984 Numerical simulations of supersonic turbulent flows. *Meeting on supernovae – O.P.M.T., Toulouse* (ed. J.-P. Zahn). Reidel.

LESIEUR, M. 1984 In *Combustion and Nonlinear phenomena* (ed. P. Clavin, B. Larrouturou & P. Pelce). Les Houches, Les éditions de Physique.

LIGHTHILL, M. J. 1952 *Proc. R. Soc. Lond.* A **211**, 564.

LIGHTHILL, M. J. 1954 *Proc. R. Soc. Lond.* A **222**, 1.

LIGHTHILL, M. J. 1955 In *Gas Dynamics of Cosmic Clouds*, IAU Symposium n° 2 (ed. H. C. van de Hulst & J. M. Burgers), p. 121. North Holland.

LIGHTHILL, M. J. 1956 In *Surveys in Mechanics* (ed. G. K. Batchelor & R. M. Davies), p. 250. Cambridge University Press.

L'VOV, V. S. & MIKHAILOV, A. V. 1978*a* *Sov. Phys., J. Exp. Theor. Phys.* **47**, 756.

L'VOV, V. S. & MIKHAILOV, A. V. 1978*b* *Sov. Phys., J. Exp. Theor. Phys.* **48**, 840.

MOISEEV, S. S., SAGDEEV, R. Z., TUR, A. V. & YANOVSKY, V. V. 1977 *Sov. Phys. Dokl.* **22**, 582.

MOISEEV, S. S., PETVIASHVILI, V. I., TUR, A. V. & YANOVSKY, V. V. 1981 *Physica* **2D**, 218.

MOISEEV, S. S., SAGDEEV, R. Z., TUR, A. V., KHOMENKO, G. A. & YANOVSKY, V. V. 1983 *Sov. Phys., J. Exp. Theor. Phys.* **58**, 1149.

PASSOT, T. 1987 Simulations numériques d'écoulements compressibles homogènes en régime turbulent: application aux nuages moléculairs. Thésis, Université de Paris VII, 14 Mai.

PASSOT, T. & POUQUET, A. 1986 *DRET-ONERA Colloquium, Poitiers, Ecole Nationale Supérieure de Mécanique et Aérotechnique.*

PASSOT, T. & POUQUET, A. 1987 Hyperviscosity for compressible flows using spectral methods. *J. Comp. Phys.* (to appear).

PELLETIER, G. 1980 *J. Plasma Phys.* **24**, 421.

POUQUET, A. 1984 In *Statistical Methods in Turbulence.* Langley Research Workshop, Applied Math. Sc., vol. 58, p. 209. Springer.

POUQUET, A., SULEM, P.-L. & MENEGUZZI, M. 1987 Influence of velocity–magnetic field correlations on decaying MHD turbulence with neutral X-points. Submitted to *Phys. Fluids.*

ROACHE, P. J. 1972 *Computational Fluid Dynamics*. Hermosa.

SAFFMAN, P. G. 1971 *Stud. Appl. Maths* **50**, 377.

STREETT, C. L., ZANG, T. A. & HUSSAINI, M. Y. 1983 Spectral Multigrid Methods with applications to transonic potential flow. ICASE *Rep.* 83-111.

SULEM, P.-L., FOURNIER, J.-D. & POUQUET, A. 1979 In *Dynamic Critical Phenomena and Related Topics*. Lecture Notes in Physics, vol. 104, p. 321. Springer.

SULEM, P.-L., FRISCH, U., POUQUET, A. & MENEGUZZI, M. 1985 *J. Plasma Phys.* **33**, 191.

TATSUMI, T. & TOKUNAGA, H. 1974 *J. Fluid Mech.* **65**, 581.

TOKUNAGA, H. 1976 *J. Phys. Soc. Japan* **41**, 328.

TOKUNAGA, H. & TATSUMI, T. 1975 *J. Phys. Soc. Japan* **38**, 1167.

WEISS, J. 1979 A class of compressible partial differential equations related to the incompressible Navier–Stokes equation. Ph.D. thesis, New York University.

WOLIBNER, W. 1933 *Math Z.* **37**, 668.

YATES, J. E. 1978 *NASA Contractor Rep.* 2987, Langley Research Center.

ZAKHAROV, V. E. & SAGDEEV, R. Z. 1970 *Sov. Phys. Dokl.* **15**, 439.